Terr. Atmos. Ocean. Sci., Vol. 28, No. 3, 517-524, June 2017 doi: 10.3319/TAO.2017.03.30.01

NOTES AND CORRESPONDENCE

Validation of the remotely sensed nighttime sea surface temperature in the shallow waters at the Dongsha Atoll

Xiaoju Pan[1, *], George T. F. Wong[2], Thomas M. DeCarlo[3], Jen-Hua Tai[2], and Anne L. Cohen[4]

[1] *Key Laboratory of Marine Chemistry Theory and Technology, Ministry of Education, Ocean University of China, Qingdao, China*
[2] *Research Center for Environmental Changes, Academia Sinica, Taipei City, Taiwan*
[3] *Massachusetts Institute of Technology/Woods Hole Oceanographic Institution Joint Program in Oceanography/Applied Ocean Physics and Engineering, and Department of Geology and Geophysics, Woods Hole Oceanographic Institution, Woods Hole, Massachusetts, USA*
[4] *Department of Geology and Geophysics, Woods Hole Oceanographic Institution, Woods Hole, Massachusetts, USA*

Article history:
Received 22 October 2016
Revised 29 March 2017
Accepted 30 March 2017

Keywords:
Sea surface temperature, Validation, Remote sensing, Dongsha Atoll, Shallow waters, Calibration

Citation:
Pan, X., G. T. F. Wong, T. M. DeCarlo, J.-H. Tai, and A. L. Cohen, 2017: Validation of the remotely sensed nighttime sea surface temperature in the shallow waters at the Dongsha Atoll. Terr. Atmos. Ocean. Sci., 28, 517-524, doi: 10.3319/TAO.2017.03.30.01

ABSTRACT

Fine scale temperature structures, which are commonly found in the top few meters of shallow water columns, may result in deviations of the remotely sensed night-time sea surface temperatures (SST) by the MODIS-Aqua sensor (SST_{sat}) from the bulk sea surface temperatures (SST_{bulk}) that they purport to represent. The discrepancies between SST_{sat} and SST_{bulk} recorded by temperature loggers at eight stations with bottom depths of 2 - 20 m around the Dongsha Atoll (DSA) between June 2013 and May 2015 were examined. The SST_{sat} had an average cool bias error of -0.43 ± 0.59°C. The bias error was larger in the warmer (> 26°C) waters which were presumably more strongly stratified. The root mean square error (RMSE) between SST_{sat} and SST_{bulk}, ±0.73°C, was 25% larger than that reported in the open northern South China Sea. An operational calibration algorithm was developed to increase the accuracy in the estimation of SST_{bulk} from SST_{sat}. In addition to removing the cool bias error, this algorithm also reduced the RMSE to virtually the same level as that found in the open northern South China Sea. With the application of the algorithm, in June 2015, the average SST in the lagoon of the DSA was raised by about 0.5°C to 31.1 ± 0.4°C, and the area of lagoon with SST_{bulk} above 31°C, the median value of the physiological temperature threshold of reef organisms, was increased by 69% to about three quarters of the lagoon.

1. INTRODUCTION

Satellite remotely sensed sea surface temperature (SST_{sat}) has been widely used synonymously as the bulk sea surface temperature (SST_{bulk}) in a wide variety of oceanographic studies (McClain 2009). However, in reality, the satellite remote sensors for SST_{sat}, such as the MODerate resolution Imaging Spectroradiometer on Aqua (MODIS-Aqua) and the Advanced Very High Resolution Radiometer (AVHRR), sense the skin temperature within the top 11 μm of the sea surface by translating the observed infrared irradiance to brightness temperature through a theoretical radiance versus blackbody temperature relationship (Walton et al. 1998; Kilpatrick et al. 2001; Donlon et al. 2002). On the other hand, SST_{bulk} is the temperature found at any depth within the first 5 - 10 m below the sea surface (Schluessel et al. 1990; Donlon et al. 2002). The inferred SST_{sat} is equivalent to SST_{bulk} only when the water column is well-mixed, and, in these cases, the agreement between the two generally falls within about -0.17 ± 0.06°C (Donlon et al. 2002). In stratified water where small scale temperature structure is present in the top few meters of the water column, they tend to differ from each other (Donlon et al. 2002). The mismatch can be a cold bias error or a warm bias error and the

* *Corresponding author*
E-mail: xpanx001@gmail.com

magnitude of these mean bias errors can vary between about -0.2 to +0.2°C (Emery et al. 2001; Li et al. 2001; Donlon et al. 2002; Barton 2007; Alvera-Azcárate et al. 2011). It is widely recognized that operational calibration algorithms are needed to bring SST_{sat} and SST_{bulk} back to agreement (Schluessel et al. 1990; Walton et al. 1998; Kilpatrick et al. 2001; Donlon et al. 2002). In shallow waters, it is highly likely that SST_{sat} and SST_{bulk} may be different from each other because the bottom reflectance in these waters may be large and this may result in small scale temperature structure in the water column. However, since the available operational calibration algorithms have been developed almost exclusively in the deep waters (Emery et al. 2001), whether they may be directly applicable to the shallow waters is questionable since the mechanism that gives rise to the temperature structures in the surface waters may be different.

Water temperature is a key environmental factor that influences the health of shallow water tropical corals (Lough 2012; Ainsworth et al. 2016). These corals frequently live close to the upper limit of their thermal tolerance so that an elevation in the water temperature by even a few degrees may significantly alter their behaviors. An accurate assessment of the water temperature that the corals are living under is necessary for evaluating the thermal stress that they are exposed to (Lough 2012; Ainsworth et al. 2016). SST_{sat} has been used for monitoring the temperature conditions associated with the world's tropical coral reefs (e.g., the NOAA Coral Reef Watch program; http://coralreefwatch.noaa.gov/satellite/index.php). Yet, this SST refers primarily to the temperature in the ambient deeper waters off the reefs where the skin temperature and the bulk temperature are similar to each other, and not to the bulk temperature in the shallow waters that the corals actually live in. The ability to directly monitor by remote sensing the bulk temperature in these shallow waters would provide more appropriate information for assessing the relationship between water temperature and the behaviors of the corals.

The Dongsha Atoll (DSA) is a shallow water tropical coral reef ecosystem located in the northern South China Sea (Fig. 1) at the northwest edge of the Coral Triangle (http://wwf.panda.org/what_we_do/where_we_work/coraltriangle/). The ambient waters surrounding the DSA, with an annual mean temperature of 26°C (~17°C in the winter and ~32°C in the summer), are warm year-round (sourced from Dongsha Atoll Research Station; http://dongsha.mr.nsysu.edu.tw). The rate of warming of these waters, about +0.02°C yr^{-1} between 1979 and 2011 is about twice of the global warming rate, about +0.01°C yr^{-1} either between 1950 and 1999 or between 2000 and 2015 (Bao and Ren 2014; Xue et al. 2016). However, the observed warming in the northern South China Sea is based primarily on satellite SST measurements, which may not accurately characterize the thermal stress to which corals on reefs in this region are exposed. Coral bleaching, a physiological response to unusually high water temperature, was evident on the DSA in 1983, 1998, and 2007 (Li et al. 2000; DeCarlo et al. 2017), but *in situ* temperature measurements are not available from that time. In an effort to use SST_{sat} to evaluate the temperature condition and the related thermal stress that the corals at the DSA are actually facing, this study attempts: (1) to evaluate the discrepancy, if any, between SST_{sat} and SST_{bulk} in the shallow waters at the DSA, and (2) if a discrepancy exists, to devise an operational calibration algorithm for minimizing the discrepancy.

2. DATA AND METHODS

2.1 Study Area

The DSA, situated at ~116.8°E, 20.7°N, is located at the shelf-edge of the northern South China Sea on the Dongsha Plateau (Fig. 1). It is almost perfectly round with a diameter of ~25 km and it covers an area of ~500 km^2. The Atoll is rimmed to the north, east and south by a broad, shallow and continuous reef, with reef-flat of up to ~3 km wide, with water depths of ~2 m, and with a total length of ~46 km. The Dongsha Island, about 2.8 km long and 0.86 km wide, is located at the western side of the DSA and it is the only part of the Atoll that is permanently above sea level. The North

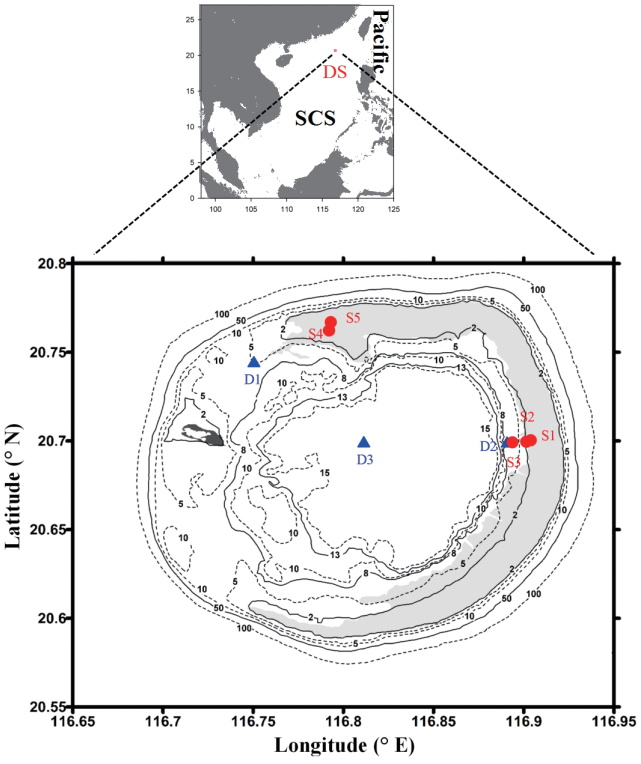

Fig. 1. Upper panel: the study area within the South China Sea (SCS); lower panel: station locations in the Dongsha Atoll (DSA). ●: shallow reef-flat stations with bottom depths of ~2 m; ▲: relatively deep stations with bottom depths ranging between ~5 and 20 m. (Color online only)

Channel and the South Channel, both about 5 - 8 m deep, to the north and the south of the Dongsha Island separate the Island from the continuous reef. The lagoon of the DSA is ~20 km wide. Its water is typically 10 - 15 m deep but the maximum depth can reach ~22 m. The water temperature in the lagoon is higher than that in the ambient water outside of the lagoon in the summer but vice versa in the winter (http://dongsha.mr.nsysu.edu.tw). In addition to exchanges through the North and South Channel at the western side of the DSA, tidal actions can also lead to exchanges between the water inside and outside of the lagoon over the reef-flat. Internal waves that are generated at the Luzon Straits propagate westward and impinge upon the DSA where they may undergo transformation and even destruction (Li et al. 2008; Alford et al. 2015; DeCarlo et al. 2015). In fact, some of the strongest internal waves in the world are found in the waters around the DSA (Zhao and Alford 2006; Farmer et al. 2011; Alford et al. 2015). The actions of these internal waves can play an important role in determining the characteristics of the water outside of the lagoon that finds its way into the lagoon (Pan et al. 2012).

2.2 Field Experiments

Between June 2013 and June 2015, *in situ* bulk water temperatures were recorded continuously for one to two years at eight stations around the DSA (Fig. 1, Table 1) by using Onset Corporation HOBO U22 temperature loggers, which had been calibrated in a constant temperature bath to an accuracy of ±0.1°C (DeCarlo et al. 2015, 2017). The locations, nominal moored depths relative to the sea surface and the time-periods of the deployment of these loggers are shown in Table 1 and Fig. 1. Of these eight stations, five (S1 through S5) were located in the shallow reef-flat with bottom depths of ~2 m, while the remaining three (D1 through D3) were either inside the lagoon or in the North Channel with bottom depths ranging between ~5 and 20 m. Each temperature logger was attached to a buoy approximately 0.5 m above the sea bed and was deployed to its nominal depth relative to the sea surface. Temperature readings were taken by the loggers at time intervals of 5 to 15 min.

2.3 Satellite Data

Daily Level-2 nighttime (4 μm) SST_{sat} data by MODIS-Aqua between 2013 and 2015, with the native spatial resolution of ~1 × 1 km^2 in the area around the DSA, were downloaded from the NASA Ocean Color Web (http://oceancolor.gsfc.nasa.gov/). Unless noted, SST_{sat} refers to the remotely sensed sea surface temperature by MODIS-Aqua in this study. The nighttime, rather than the daytime, SST_{sat} was used in order to minimize the effects of solar heating, reflected radiation, sensible heat loss and/or surface evaporation on the remotely sensed skin temperature (Schluessel et al. 1990). The SST_{sat} data were validated by comparing them to the SST_{bulk} records following the protocols of Bailey and Werdell (2006). The SST_{sat} product in the highest quality level (q0), passing all of the pre-defined threshold tests, was used. The pixels were masked after atmospheric correction by any of the following flags: land, cloud or ice, high top-of-atmosphere radiance, stray light, sun glint, or atmospheric correction failure (Brown and Minnett 1999). The 3 × 3 pixel arrays centered on the field stations, each with ~1 km resolution (sensor native), were analyzed. The arithmetic mean and the standard deviation (SD) of the non-masked pixels in each 3 × 3 box were determined. To minimize the effect of outliers, which would partly be associated with the heterogeneous distribution of SST in space, any pixels whose values were beyond 1.5 SD of the arithmetic mean were filtered. The filtered arithmetic mean for the rest non-masked pixels was determined and reported as SST_{sat}. A time-window of ±15 min between the satellite overpass and the field *in situ* observations was allowed. With such a narrow time-window, any temporal mismatch between the two sources of data should be almost negligible. The goodness-of-fit between SST_{sat} and SST_{bulk} is assessed by the mean bias error (MBE) and the root mean square error (RMSE) such that:

$$MBE = \sum(SST_{sat} - SST_{bulk})/n \quad (1)$$

$$RMSE = \pm\sqrt{\sum(SST_{sat} - SST_{bulk})^2/n} \quad (2)$$

Here, n represents the number of match-up observations.

3. RESULTS AND DISCUSSIONS

3.1 Discrepancy Between SST_{sat} and SST_{bulk} at the DSA

The relationship between SST_{sat} and SST_{bulk} at the eight stations at the DSA is shown in Fig. 2. A strong positive correlation (r = 0.980) between the two was clearly evident, indicating that SST_{sat} could represent SST_{bulk} well. However, most (~82%) of the data points fell below the 1:1 line, indicating that there was a cool bias error in SST_{sat}. Furthermore, below 26°C, which corresponded approximately to the mean annual SST, the data points tended to cluster closer together. At higher temperatures, the data points, on average, seemed to fall farther below the 1:1 line, indicating a larger cool bias error, and the scatter became larger. Thus, there could have been a temperature dependence in the deviations of SST_{sat} from SST_{bulk} as well as the uncertainty of the former relative to the latter. These results are consistent with the increasing likelihood that an increasingly well-defined small scale temperature structure may be present in the first few meters of these shallow water columns as the surface temperature increases so that SST_{sat} and SST_{bulk} may be increasingly different from each other.

Table 1. Temperature loggers deployed in the waters around the Dongsha Atoll.

Station	location	Depth* (m)	Deployment period
S1	Reef-flat	1	6/21/2013-6/4/2015
S2	Reef-flat	2	6/26/2013-5/31/2015
S3	Reef-flat	1	6/19/2013-5/23/2014
S4	Reef-flat	0.5	6/19/2013-6/17/2014
S5	Reef-flat	1	6/19/2013-5/29/2015
D1	N Channel	4	6/20/2013-5/29/2015
D2	Lagoon	1	6/19/2013-5/30/2015
D3	Lagoon	5	6/24/2014-5/29/2015

*Note: *: Moored depth of the temperature logger relative to the sea surface.*

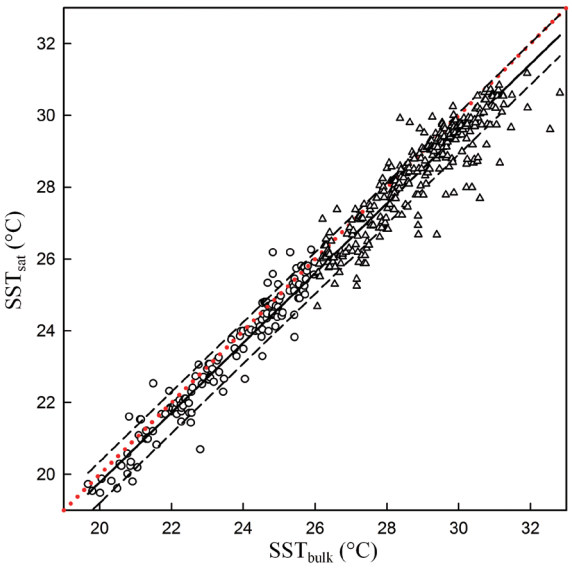

Fig. 2. Relationship between remotely sensed SSTs by MODIS-Aqua, SST_{sat}, and the field observed bulk sea surface temperatures, SST_{bulk}, in the waters at the DSA. ○, △: data points at SST_{bulk} below and above 26°C, respectively; dotted line (red): 1:1 relationship; solid line: best-fit linear (Model II) regression; dashed lines: SST_{sat} deviated by one RMSE from the best-fit regression. (Color online only)

The results of a statistical analysis of the relationship between SST_{sat} and SST_{bulk} are shown in Table 2. The mean bias error (MBE) indicated an average cool bias error of -0.43 ± 0.59°C (n = 466) in SST_{sat} (Fig. 3a, Table 2). This value was substantially larger than the range of the cool bias errors, about -0.1 to -0.2°C, found in deeper water columns (Donlon et al. 2002; Barton 2007; Alvera-Azcárate et al. 2011) and it should be taken into account in studying the behaviors of corals as the corals respond to temperature changes of even a few degrees (Lough 2012). The RMSE between SST_{sat} and SST_{bulk} in these shallow waters in the DSA, ±0.73°C, was larger than that, ±0.59°C, reported in the open northern South China Sea by about 25% (Pan et al. 2015). The frequency distribution of the deviations of SST_{sat} from SST_{bulk} indicates that ~80% of the deviations were within ±1 SD from the MBE, between -1.0 and 0.2°C (Fig. 3a). Most (6 of 8) of the biases exceeding 3 SD from the MBE were cool biases (bias error < -2.2°C). Only in two remaining cases were the biases the warm biases (bias error > 1.3°C). As a result, the skewness was -1.02, while the kurtosis was 3.11 (Table 2).

The variability in the relationship between SST_{sat} and SST_{bulk} was evaluated by comparing the results in the statistical analyses of sub-sets of the data set. Year-to-year variation was not obvious. The MBE for the data between June 2013 and May 2014, -0.40 ± 0.60°C, and between June 2014 and May 2015, -0.45 ± 0.59°C, were not statistically different from each other (P = 0.360), nor was their RMSE, skewness or kurtosis (Table 2).

Within the range of depths of the water-column that the temperature loggers were moored, there was also no obvious depth dependence in the relationship between SST_{sat} and SST_{bulk}. The MBE of SST_{sat} relative to SST_{bulk} measured in the reef-flat in water-column depths of ~2 m, -0.40 ± 0.61°C, and that relative to SST_{bulk} in the lagoon and channel in water-column depths of 5 - 20 m, -0.46 ± 0.58°C, were not significantly different from each other (P = 0.271). The corresponding RMSE and skewness were also reasonably similar to each other, and the kurtosis was larger in the latter group (Table 2).

In contrast, the temperature dependence in the relationship between SST_{sat} and SST_{bulk} was statistically significant. The MBE at SST_{bulk} below 26°C, -0.27 ± 0.45°C, was significantly different (P < 0.001) from that, -0.50 ± 0.64°C, at SST_{bulk} above 26°C (Fig. 3b, Table 2). The corresponding RMSE in the former group, ±0.52°C, was smaller than that, ±0.81°C, in the latter group (Table 2). The SST of 26°C also approximately separates the water temperature in the area in November through April during the northeast monsoonal season from that in the remainder of the year. Thus, SST_{sat} is less accurate in depicting SST_{bulk} in the warm summer months when it is most needed for assessing the effect of water temperature on the behaviors of the corals in the DSA.

3.2 Operational Calibration Algorithm for Reducing the Discrepancies Between SST_{sat} and SST_{bulk}

The relationship between SST_{sat} and SST_{bulk} may be represented as a linear relationship in a Model II regression analysis (Fig. 2) such that:

$$SST_{sat} = (0.354 \pm 0.249) + (0.971 \pm 0.009)\,SST_{bulk} \quad (r^2 = 0.960,\ n = 466) \tag{3}$$

The high correlation coefficient indicates that the equation can represent the relationship well. The associated RMSEs

Table 2. Statistical results of the match-up comparisons between SST_{sat} and SST_{bulk}.

Parameter*	All	Yearly periods		Bottom depth (m)		SST_{bulk} (°C)		linear calibration+		
		6/2013 - 5/2014	6/2014 - 5/2015	~ 2	5 - 20	< 26	> 26	All	SST_{bulk} < 26°C	SST_{bulk} > 26°C
n	466	219	247	234	232	154	312	466	154	312
Min BE (°C)	-2.93	-2.90	-2.93	-2.90	-2.93	-2.10	-2.93	-2.02	-1.72	-2.02
Max BE (°C)	1.56	1.56	1.36	1.56	1.05	1.36	1.56	2.37	1.80	2.37
Median BE (°C)	-0.33	-0.34	-0.33	-0.33	-0.33	-0.25	-0.40	-0.08	-0.06	-0.10
MBE (°C)	-0.43	-0.40	-0.45	-0.40	-0.46	-0.27	-0.50	0.00	-0.06	0.03
SD of MBE (°C)	0.59	0.60	0.59	0.61	0.58	0.45	0.64	0.58	0.45	0.63
RMSE (°C)	±0.73	±0.72	±0.74	±0.72	±0.73	±0.52	±0.81	±0.58	±0.46	±0.63
Skewness	-1.02	-0.93	-1.11	-0.75	-1.34	-0.11	-1.02	0.52	0.09	0.99
Kurtosis	3.11	3.34	2.97	2.42	3.95	3.16	2.41	3.61	2.95	2.25

*Note: *: n: number of match-up data; min, max, and median BE: minimum, maximum, and median bias error; MBE: mean bias error; RMSE: root mean square error. + SST_{sat} was estimated from SST_{bulk} by using the linear function of Eq. (3).*

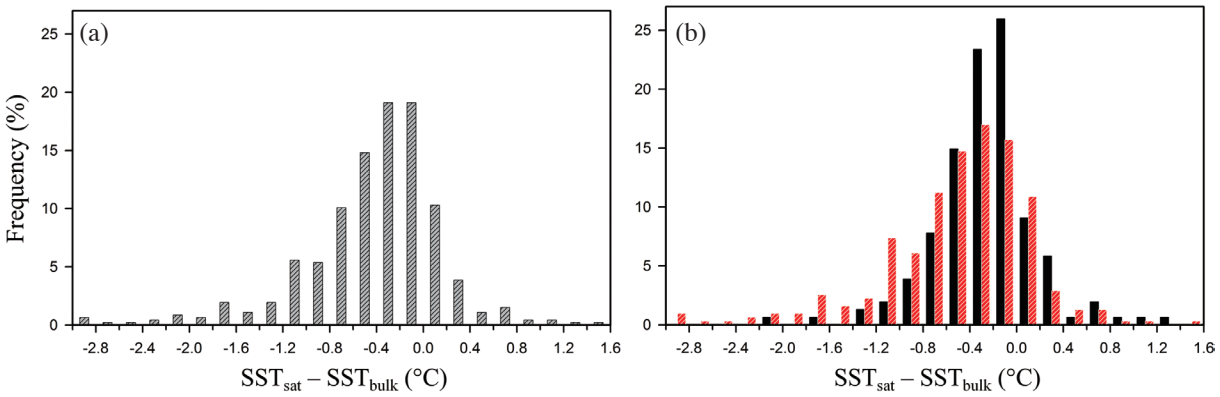

Fig. 3. Frequency distribution diagram in the deviation of SST_{sat} from SST_{bulk}. (a) All data points; (b) data points at SST_{bulk} below (black) and above 26°C (red). (Color online only)

were ±0.58, ±0.46, and ±0.63°C for the dataset as a whole and at SST_{bulk} below and above 26°C, respectively (Table 2). By applying this operational calibration algorithm to SST_{sat}, in addition to removing the cool bias error, the RMSE between SST_{sat} and SST_{bulk} was reduced to a value, ±0.58°C, which is virtually identical to that, ±0.59°C, found in the open northern South China Sea (Pan et al. 2015). In practice, SST_{bulk} is estimated from SST_{sat} and Eq. (3) may be transformed into:

$$SST_{bulk} = -0.365 + 1.030 SST_{sat} \quad (4)$$

Among the eight stations, S1 and S2, D2 and S3, and S4 and S5 were located within 1 km from each other so that these pairs of station might have fallen within a single remotely sensed pixel. Thus, alternatively, the synchronous average SST_{bulk} at these three pairs of stations plus the SST_{bulk} at stations D1 and D3 could be used to construct the relationship between SST_{bulk} and SST_{sat}. The resulting relationship was:

$$SST_{sat} = (0.384 \pm 0.275) + (0.970 \pm 0.010) SST_{bulk} \quad (r^2 = 0.964, n = 347) \quad (5)$$

This relationship was not significantly different from Eq. (3) when the eight stations were treated as individual stations. Nevertheless, the RMSE in Eq. (5), ±0.44°C, was slightly smaller than that, ±0.58°C, in Eq. (3). Furthermore, within each pair of the nearby stations, the SST_{bulk} recorded synchronously by the two sensors could differ significantly, e.g., > 2°C in some occasions, from each other. As a result, SST_{bulk} in S1, S3, and S5 were statistically (paired t-test $P < 0.001$) lower than those in S2, D2, and S4 by 0.11, 0.08, and 0.14°C, respectively, and the synchronous average SST_{bulk} would have been more similar to the SST_{sat}, which was the average temperature over the entire pixel. The lower RMSE and the difference in SST_{bulk} at the nearby stations were consistent with this effect of small scale spatial variations in SST_{bulk} within the pixel area of 1 × 1 km^2. Since, in practice, the SST_{sat} is likely used to represent a single observation

within a pixel, using Eq. (3) to estimate SST_{bulk} and claiming a higher RMSE would be more prudent.

Separating the dataset into sub-data groups with SST_{bulk} above and below 26°C and then developing the relationship between SST_{sat} and SST_{bulk} in each sub-group separately did not reduce the RMSE. In each case, the relationship could be represented by a linear equation such that:
at $SST_{bulk} < 26$°C:

$$SST_{sat} = (-1.586 \pm 0.511) + (1.056 \pm 0.022)\, SST_{bulk} \quad (r^2 = 0.939, n = 154) \tag{6a}$$

at $SST_{bulk} > 26$°C:

$$SST_{sat} = (-0.019 \pm 0.754) + (0.983 \pm 0.026)\, SST_{bulk} \quad (r^2 = 0.819, n = 312) \tag{6b}$$

While these equations can represent the relationship well as indicated by their reasonably high correlation coefficients, these coefficients were actually lower than that, 0.960, when Eq. (3) was used to represent the relationship through the complete temperature range. Furthermore, by using these two equations, the RMSEs at SST_{bulk} below and above 26, ±0.45, and ±0.63°C, were identical to those, ±0.46 and ±0.63°C, when Eq. (3) was used. Thus, using Eq. (3) for the operational calibration algorithm is preferred and chosen here. With appropriate regional tuning, the SST_{bulk} may be similarly calibrated in other shallow waters.

3.3 Application of the Operational Calibration Algorithm - SST at the DSA in June 2015

The distributions of SST in the DSA in June 2015 without and with the application of the operational calibration algorithm are shown in Fig. 4. Qualitatively, similar major distributional patterns were depicted in both cases. Thus, the coldest waters were found along the fore-reef and the reef-flat, where cold subsurface water might have been uplifted to the surface and washed over the reef-flat by the combined actions of the incoming and breaking internal waves, and tides (Pan et al. 2012; DeCarlo et al. 2015). The signal was especially prominent at the eastern and northeastern fore-reef and reef-flat, which were in the direct path of propagation of the internal waves. The intrusion of colder offshore waters into the lagoon through the channels was indicated by the two tongues of colder waters that extended from the offshore into the lagoon north and south of the Dongsha Island. On the other hand, in a phenomenon that relates to a specific SST, the application of the operational calibration algorithm could lead to significantly different interpretations. Lough (2012) reported that the physiological processes of reef organisms may be compromised at temperatures above 30 to 32°C. Taking the average temperature in this range, 31°C, as an indicating temperature, without applying the operational calibration algorithm, the average SST in the lagoon was 30.6 ± 0.4°C and the SST in 4% of its area was above 31°C (Fig. 4a). When the operational calibration algorithm was applied, the average SST in the lagoon was 31.1 ± 0.4°C and the fraction of its area where SST was above 31°C became 73% (Fig. 4b). The SST was especially elevated in the eastern half of the lagoon east of about 116.8°E. In this sub-section in the lagoon, without applying the algorithm, the average SST was 30.7 ± 0.3°C and 7% of its area was above 31°C. When the algorithm was applied, the average SST increased to 31.3 ± 0.3°C and 89% of its area was above 31°C. Thus, the application of the operational calibration algorithm led to a significant increase, 0.5°C, in the monthly average SST in the lagoon, and a dramatic increase, 69%, in the fraction of the area of the lagoon with a temperature above 31°C, the median value of the physiological temperature threshold of reef organisms. In fact, the SST in virtually three quarters

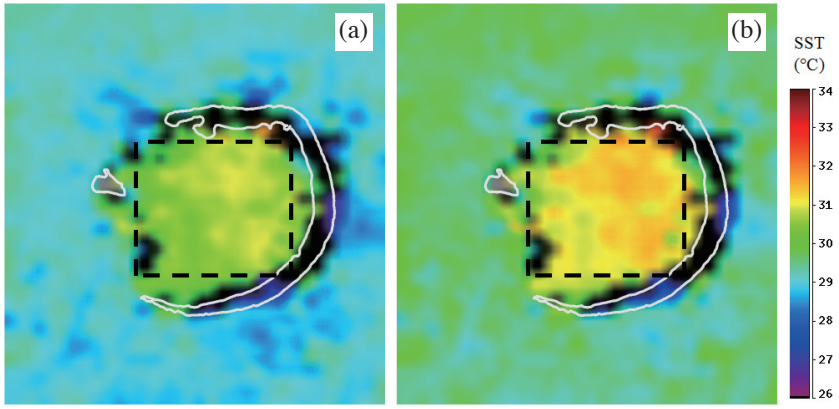

Fig. 4. Monthly average distributions in SST_{sat} in June 2015. (a) Without and (b) with the application of the operational calibration algorithm by using Eq. (4). White lines: the 2-m isobaths; black dashed-line box: area used for calculating the statistics in the lagoon. (Color online only)

of the lagoon was above 31°C. Visual surveys of the coral ecosystem at various locations in the lagoon of the DSA, including Station D3 (Fig. 1), indicated that, while there was no evidence of bleaching of the corals in prior to early June, extensive bleaching was found by late July (DeCarlo et al. 2017). These observations were consistent with the elevated SST_{bulk} in the lagoon in June that was derived from SST_{sat} after the operation calibration algorithm had been applied.

4. SUMMARY

Satellite remotely sensed SST by MODIS-Aqua, SST_{sat}, has a cool bias error of -0.43 ± 0.59°C in the shallow waters at the DSA. The uncertainty in SST_{sat}, ±0.73°C, is larger than that, ±0.59°C, in the ambient water in the adjoining northern South China Sea. The bias error is larger in the warmer waters, where stratification is likely to be stronger, at temperatures above 26°C. This cool bias error can be removed with an operation calibration algorithm, which can also reduce the uncertainty in SST_{sat} to ±0.58°C.

Acknowledgements This work was supported in part by the Key Research and Development Program of Shandong Province (grant no. 2015GSF117017) and Ocean University of China (grant no. 201513037 and 201512011) to Pan, and the Academia Sinica through grant titled "Ocean Acidification: Comparative biogeochemistry in shallow-water tropical coral reef ecosystems in a naturally acidic marine environment" to Wong. This is MCTL Contribution No. 136.

REFERENCES

Ainsworth, T. D., S. F. Heron, J. C. Ortiz, P. J. Mumby, A. Grech, D. Ogawa, C. M. Eakin, and W. Leggat, 2016: Climate change disables coral bleaching protection on the Great Barrier Reef. *Science*, **352**, 338-342, doi: 10.1126/science.aac7125. [Link]

Alford, M. H., T. Peacock, J. A. MacKinnon, J. D. Nash, M. C. Buijsman, L. R. Centuroni, S. Y. Chao, M. H. Chang, D. M. Farmer, O. B. Fringer, K. H. Fu, P. C. Gallacher, H. C. Graber, K. R. Helfrich, S. M. Jachec, C. R. Jackson, J. M. Klymak, D. S. Ko, S. Jan, T. M. S. Johnston, S. Legg, I. H. Lee, R. C. Lien, M. J. Mercier, J. N. Moum, R. Musgrave, J. H. Park, A. I. Pickering, R. Pinkel, L. Rainville, S. R. Ramp, D. L. Rudnick, S. Sarkar, A. Scotti, H. L. Simmons, L. C. St Laurent, S. K. Venayagamoorthy, Y. H. Wang, J. Wang, Y. J. Yang, T. Paluszkiewicz, and T. Y. D. Tang, 2015: The formation and fate of internal waves in the South China Sea. *Nature*, **521**, 65-69, doi: 10.1038/nature14399. [Link]

Alvera-Azcárate, A., C. Troupin, A. Barth, and J. M. Beckers, 2011: Comparison between satellite and in situ sea surface temperature data in the Western Mediterranean Sea. *Ocean Dyn.*, **61**, 767-778, doi: 10.1007/s10236-011-0403-x. [Link]

Bailey, S. W. and P. J. Werdell, 2006: A multi-sensor approach for the on-orbit validation of ocean color satellite data products. *Remote Sens. Environ.*, **102**, 12-23, doi: 10.1016/j.rse.2006.01.015. [Link]

Bao, B. and G. Ren, 2014: Climatological characteristics and long-term change of SST over the marginal seas of China. *Cont. Shelf Res.*, **77**, 96-106, doi: 10.1016/j.csr.2014.01.013. [Link]

Barton, I. J., 2007: Comparison of in situ and satellite-derived sea surface temperatures in the Gulf of Carpentaria. *J. Atmos. Ocean. Technol.*, **24**, 1773-1784, doi: 10.1175/JTECH2084.1. [Link]

Brown, O. B. and P. J. Minnett, 1999: MODIS Infrared Sea Surface Temperature Algorithm - Algorithm Theoretical Basis Document, version 2.0. Available at http://modis.gsfc.nasa.gov/data/atbd/atbd_mod25.pdf.

DeCarlo, T. M., K. B. Karnauskas, K. A. Davis, and G. T. F. Wong, 2015: Climate modulates internal wave activity in the Northern South China Sea. *Geophys. Res. Lett.*, **42**, 831-838, doi: 10.1002/2014GL062522. [Link]

DeCarlo T. M., A. L. Cohen, G. T. F. Wong, K. A. Davis, P. Lohmann, and K. Soong, 2017: Mass coral mortality under local amplification of 2°C ocean warming. *Scientific Reports*, **7**, 44586, doi: 10.1038/srep44586. [Link]

Donlon, C. J., P. J. Minnett, C. Gentemann, T. J. Nightingale, I. J. Barton, B. Ward, and M. J. Murray, 2002: Toward improved validation of satellite sea surface skin temperature measurements for climate research. *J. Climate*, **15**, 353-369, doi: 10.1175/1520-0442(2002)015<0353:TIVOSS>2.0.CO;2. [Link]

Emery, W. J., S. Castro, G. A. Wick, P. Schluessel, and C. Donlon, 2001: Estimating sea surface temperature from infrared satellite and in situ temperature data. *Bull. Amer. Meteorol. Soc.*, **82**, 2773-2785, doi: 10.1175/1520-0477(2001)082<2773:ESSTFI>2.3.CO;2. [Link]

Farmer, D. M., M. H. Alford, R. C. Lien, Y. J. Yang, M. H. Chang, and Q. Li, 2011: From Luzon Strait to Dongsha Plateau: Stages in the life of an internal wave. *Oceanography*, **24**, 64-77, doi: 10.5670/oceanog.2011.95. [Link]

Kilpatrick, K. A., G. P. Podesta, and R. Evans, 2001: Overview of the NOAA/NASA advanced very high resolution radiometer Pathfinder algorithm for sea surface temperature and associated matchup database. *J. Geophys. Res.*, **106**, 9179-9197, doi: 10.1029/1999JC000065. [Link]

Li, J. J., T. F. Lee, K. S. Tew, and L. S. Fang, 2000: Changes in the coral community at Dong-sha Atoll, South China Sea from 1975 to 1998. *Acta Zoologica Taiwanica*, **11**, 1-15, doi: 10.6576/AZT.2000.11.(1).1. [Link]

Li, X., W. Pichel, P. Clemente-Colon, V. Krasnopolsky, and

J. Sapper, 2001: Validation of coastal sea and lake surface temperature measurements derived from NOAA/AVHRR Data. *Int. J. Remote Sens.*, **22**, 1285-1303, doi: 10.1080/01431160151144350. [Link]

Li, X., Z. Zhao, and W. G. Pichel, 2008: Internal solitary waves in the northwestern South China Sea inferred from satellite images. *Geophys. Res. Lett.*, **35**, L13605, doi: 10.1029/2008GL034272. [Link]

Lough, J. M., 2012: Small change, big difference: Sea surface temperature distributions for tropical coral reef ecosystems, 1950-2011. *J. Geophys. Res.*, **117**, C09018, doi: 10.1029/2012JC008199. [Link]

McClain, C. R., 2009: A decade of satellite ocean color observations. *Annu. Rev. Mar. Sci.*, **1**, 19-42, doi: 10.1146/annurev.marine.010908.163650. [Link]

Pan, X., G. T. F. Wong, F. K. Shiah, and T. Y. Ho, 2012: Enhancement of biological productivity by internal waves: Observations in the summertime in the northern South China Sea. *J. Oceanogr.*, **68**, 427-437, doi: 10.1007/s10872-012-0107-y. [Link]

Pan, X., G. T. F. Wong, J. H. Tai, and T. Y. Ho, 2015: Climatology of physical hydrographic and biological characteristics of the northern South China Sea Shelf-sea (NoSoCS) and adjacent waters: Observations from satellite remote sensing. *Deep-Sea Res. Part II-Top. Stud. Oceanogr.*, **117**, 10-22, doi: 10.1016/j.dsr2.2015.02.022. [Link]

Schluessel, P., W. J. Emery, H. Grassl, and T. Mammen, 1990: On the bulk-skin temperature difference and its impact on satellite remote sensing of sea surface temperature. *J. Geophys. Res.*, **95**, 13341-13356, doi: 10.1029/JC095iC08p13341. [Link]

Walton, C. C., W. G. Pichel, J. F. Sapper, and D. A. May, 1998: The development and operational application of nonlinear algorithms for the measurement of sea surface temperatures with the NOAA polar-orbiting environmental satellites. *J. Geophys. Res.*, **103**, 27999-28012, doi: 10.1029/98JC02370. [Link]

Xue, Y., Z. Z. Hu, A. Kumar, V. Banzon, B. Huang, and J. Kennedy, 2016: Sea surface temperatures [in "State of the Climate in 2013"]. *Bull. Amer. Meteorol. Soc.*, **97**, S63-S66.

Zhao, Z. and M. H. Alford, 2006: Source and propagation of internal solitary waves in the northeastern South China Sea. *J. Geophys. Res.*, **111**, C11012, doi: 10.1029/2006JC003644. [Link]